Available online at www.sciencedirect.com
ScienceDirect
ELSEVIER
Palaeogeography, Palaeoclimatology, Palaeoecology 241 (2006) 515–530
PALAEO
www.elsevier.com/locate/palaeo

Controls on carbonate and terrigenous deposition in the incipient Benguela upwelling system during the middle to the late Miocene (ODP Sites 1085 and 1087)

Mia Maria Kastanja [a,*], Bernhard Diekmann [b], Rüdiger Henrich [c]

[a] *Research Center Ocean Margin – University of Bremen, P.O. Box 33040, 28324 Bremen, Germany*
[b] *Alfred Wegener Institute for Polar and Marine Research, 14473 Potsdam, Germany*
[c] *Faculty of Geosciences, FB.5, University of Bremen, P.O. Box 30440, 28334 Bremen, Germany*

Received 8 March 2005; received in revised form 11 April 2006; accepted 5 May 2006

Abstract

This study deals with the variability of biogenic carbonate and terrigenous depositional patterns in the Cape Basin area of the South Atlantic during the middle to the late Miocene focusing on ODP Sites 1085 and 1087 sediments at the Benguela Upwelling area, Southwest Africa. The investigations are based on grain-size analysis and clay mineralogy. The sedimentary records at both sites provide information about climate and environmental changes. The direct input of terrigenous material from southwestern Africa is driven by a complex interaction of river and wind transport, and ocean currents. The considerable amount of dust input derived from the Namib Desert started to become important after 11.2 Ma, pointing to an increased supply of cool intermediate waters to mid-latitude surface waters in the upwelling regions, which coincided with the establishment of the wind-driven Benguela upwelling system. A major drop in $CaCO_3$ concentration between 10.4 and 10.1 Ma is caused mainly by changes in calcareous nannoplankton production, while another drop between 9.6 and 9 Ma is triggered by a combination of production changes of calcareous nannoplankton and dilution, in response to high shelf supply during global lowering of the sea level.

Keywords: Silt analysis; Clay mineralogy; Benguela upwelling; Miocene

1. Introduction

In the course of the Cenozoic climate deterioration, the climate system of the middle to the late Miocene was particularly affected by the expansion of Antarctic ice sheets, the cooling of surface and deep water masses, aridification of continents, as well as tectonic processes leading to the emergence of the Panama Isthmus and the uplift of Alpine orogens, such as the Himalaya Mountains and the Tibetan Plateau (e.g., Kennett et al., 1985; Haq et al., 1987; Wright and Miller, 1996; Zachos et al., 2001a,b).

These changing boundary conditions had a significant impact on ocean circulation, nutrient supply and, thus, on the biological productivity of the oceans. Between 12 and 9 Ma, some major drops in $CaCO_3$

* Corresponding author.
E-mail address: kastanja@uni-bremen.de (M.M. Kastanja).

0031-0182/$ - see front matter © 2006 Elsevier B.V. All rights reserved.
doi:10.1016/j.palaeo.2006.05.004

concentration occurred in the central and eastern Pacific (Lyle et al., 1995; Farrel et al., 1995), Ceara Rise (King et al., 1997), and the Caribbean Sea (Roth et al., 2000). So far, deep-water circulation changes, shoaling of the Carbonate Compensation Depth (CCD), and dissolution process were generally believed as possible causes of this so-called "Carbonate Crash" event. Recently, this event has also been described in the southeast Atlantic Ocean (Diester-Haass et al., 2004; Westerhold et al., 2005; Krammer et al., 2006). According to Diester-Haass et al. (2004), major increases in clastic input via the Orange River during the global sea-level regressions formed the principle cause of the carbonate crash in the Southeast Atlantic, whereas carbonate dissolution as reflected on benthic/planktonic (B/P) ratios of foraminifers is not related to the carbonate drops. Their study is based on the concentrations of terrigenous particles in the >40 μm size fraction and abundance of >63 μm shelf-derived particles as proxies of total clastic delivery and transport energy. However, coarse fractions only give small contribution (<5% of total sediment) to the bulk sediment, which is dominated by nannofossil ooze and terrigenous clay fraction (Wefer et al., 1998). In contrast to the findings from Diester-Haass et al. (2004), Krammer et al. (2006) proposed, based on calcareous nannoplankton evidence, that the major $CaCO_3$ depression was rather controlled by variation in nannofossil carbonate production than by dilution of terrigenous material.

Although the causes of the middle Miocene 'Carbonate Crash' events along the western continental margin of South Africa has been investigated in much detail (Diester-Haass et al., 2004; Krammer et al., 2006), our knowledge on the variability of the sedimentary process in this area is not fully understood. In this study, we aim at contributing new aspects to the understanding of the variability of the sedimentary processes in this area and their driving forces by means of analysing clay mineralogy, geochemistry and grain-size distribution from deep-sea sediment of SW Africa (ODP Sites 1085 and 1087). Furthermore, this study is intended to give new insights into the controlling factors on sediment deposition during the middle to the late Miocene in relation to the 'Carbonate Crash' event and the development of the Benguela upwelling. Detailed investigations of both terrigenous and calcareous sediment fraction clearly bear a high potential to evaluate controls on sediment transport and variation in production of pelagic carbonates. Because of their proximity to the continent, the sediment records at both positions are very useful in detecting upwelling signals, changes in biogenic carbonate deposition, and preservation, as well as in the sources of terrigenous sediment input, by fluvial (Orange River) and aeolian (Namib Desert) supplies.

2. Background and regional setting

The Benguela upwelling system (Benguela Current) carries the northward flowing, cold, upwelled water found at the western coast of South Africa and Namibia (SW Africa) between 15°S and 34°S (Siesser, 1978). This system is characterized by high productivity (>180 g C/m^2/yr) and high sedimentation rates (Berger, 1989). Today, the Benguela Current is the eastern boundary current of the South Atlantic subtropical gyre (Peterson and Stramma, 1991).

The middle to late Miocene expansion of ice-sheets on Antarctica and associated changes in deep-water circulation gave rise to increased latitudinal climate gradients that also affected low-latitude processes on the southern hemisphere. The supply of cool intermediate waters to mid-latitude surface waters in the upwelling regions progressively decreased moisture levels in the atmosphere in the hinterland (Flower and Kennet, 1995), which established the initiation of the Benguela upwelling and the formation of the Namib Desert (Siesser, 1978). Accordingly, aridification in southern Africa is documented at 10 Ma from isotope and geochemical studies in the Walvis Bay (Partridge, 1993), Meteor Rise (Site 1088) at 9.7 Ma from a clay mineral study (Diekmann et al., 2003), and Cape Basin at 9.6 Ma based on the oxygen isotope record at Site 1085 (Westerhold et al., 2005). This coincided with the first establishment of the trade-wind-driven Benguela upwelling system around 10 Ma (Hay and Brock, 1992). Furthermore, Diester-Haass et al. (1990, 1992) have postulated a northward shift of the Benguela Current since the middle Miocene that might have strengthened upwelling at about 10.5 Ma.

Three main transport agents supply detrital sediment from land to the ocean along the Southwest African margin: river discharge, ocean currents, and aeolian input. The Orange River is the only perennial river of SW Africa. It carries high volumes of mud suspension southward into the South Atlantic where it is further dispersed by the prevailing bottom currents (Van der Merwe and Heystek, 1955; Chester et al., 1971, 1972; Summerhayes et al., 1995). The Namib Desert is a coastal strip desert with very strong winds, especially in the south near Lüderitz (Rogers, 1977; Bremner, 1978). Grain-size studies on Quaternary sediments from the Walvis Ridge show that the aeolian dust export from Namib Desert to the South West African margin is

almost exclusively supplied by the SE trade wind (Stuut et al., 2002).

3. Material and methods

3.1. Sites 1085 and 1087

ODP Sites 1085 and 1087 were drilled in the Cape Basin. Site 1085 (29°22.47′S, 13°59.41′E, 1713 m water depth) is located at the southwestern African continental margin, beneath the southern part of the Benguela Current upwelling region off the mouth of the Orange River (Fig. 1). Site 1087 is situated in the southernmost Cape Basin (31°27.91′S, 15°18.65′E, 1372 m water depth) (Fig. 1). Today, both sites are bathed primarily in Upper Circumpolar Deep Water (UCDW) near the mixing zone with the North Atlantic Deep Water (NADW). The sediments in the entire studied section at both sites consist mainly of nannofossil ooze (Wefer et al., 1998) with the linear sedimentation rates (LSR) ranging from 2 to 7 cm/ka (Westerhold et al., 2005).

WE selected sediment sequences from both sites from the middle to late Miocene interval. At Site 1085 Hole A samples were taken from cores 43X to 61X (399–569 mbsf), with sample spaces ranging between 50 and 100 cm. The resolution for the whole section thus ranges between 8 and 100 ka. At Site 1087, samples were taken from 310 mbsf to 405 mbsf (cores 35X to 44X). This site covers the time interval of the late Miocene only. Sample spacing ranges between 100 and 200 cm, providing an average resolution of 40 ka.

3.2. Age model and mass accumulation rates

The age model and the bulk mass accumulation rate (MAR bulk) calculations were provided by Westerhold et al. (2005). The age model was generated by orbital tuning of a high-resolution composite XRF-Fe intensity record of ODP Sites 1085 and 1087 to an Eccentricity–

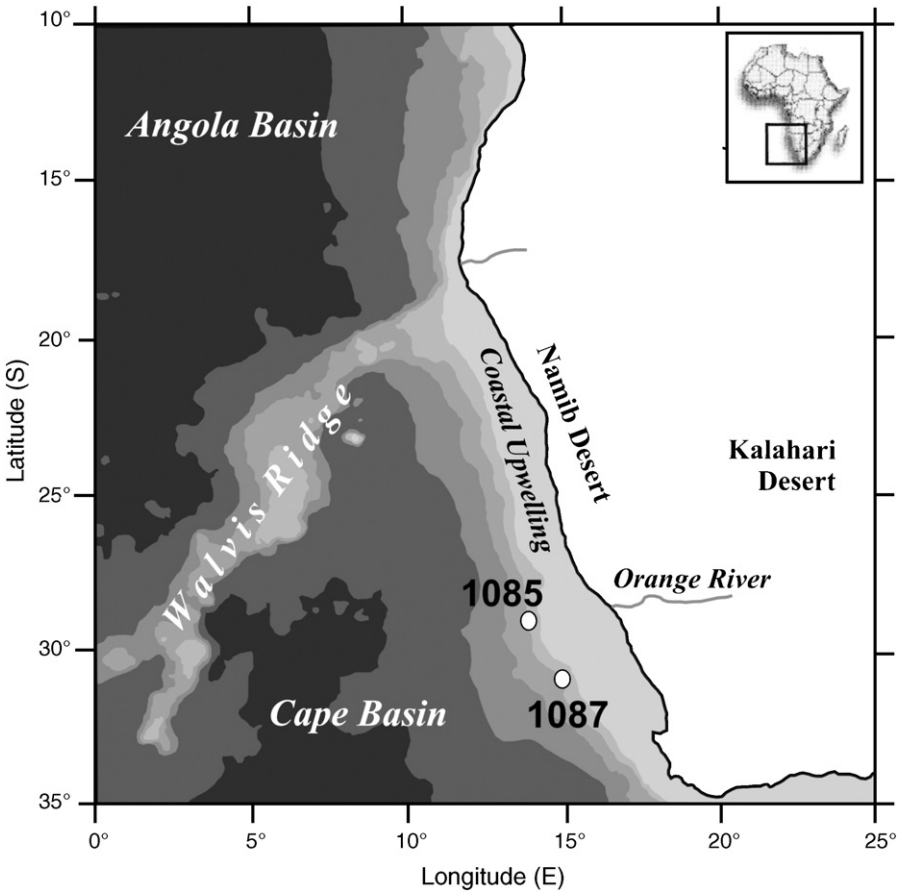

Fig. 1. Location of ODP Sites 1085 (1713 m) and 1087 (1371 m) on the continental slope of the Cape Basin, southeast Atlantic. Grey to black shading illustrates the bathymetric depth. Map is redrawn from Stuut et al. (2002).

Tilt–Precession (ETP) target curve (Westerhold et al., 2005). MAR of individual components was calculated by multiplying the MAR bulk with the proportion of the respective sediment component.

3.3. Analytical procedure

For the grain-size analyses, ~20 cm^3 sample was split into three grain-size fraction, sand (>63 μm), silt (2–63 μm) and clay (<2 μm). The relative proportions of each fraction were then determined. Furthermore, the lithogenic and biogenic silt components have been investigated following the standard technique of McCave et al. (1995a). To determine the particle size of the silt fraction, a Micromeritics Sedigraph 5100 was used over the 0.1 to 63 μm ranges. In this study we employ the grain-size analysis on terrigenous silt fraction to emphasize the variation of paleo bottom-current strength and dust input. Besides, the grain-size analysis on calcareous silt fraction allows us to distinguish the larger juvenile foraminifers and foraminiferal fragments from smaller nannofossil placoliths by a clear minimum of both constituents at a modal grain size of 8 μm (Frenz et al., 2005).

About 1 g of the freeze-dried bulk sediment and clay fraction samples were set aside for total carbon (TC) determination, measured with a LECO-CS 200 elemental analyzer. This device also quantifies total organic carbon (TOC) contents after removing the carbonate using HCl. The $CaCO_3$ concentration was then calculated using the following equation:

$$CaCO_3 = (TC - TOC) * 8.33.$$

The clay fraction was analyzed for the four main clay mineral groups kaolinite, smectite, illite, and chlorite following standard procedures of Petschick et al. (1996). The proportions of each mineral were calculated semi-quantitatively from weighted XRD peak areas (Biscaye, 1965). Additionally, illite chemistry was assessed using the ratio of integrated 5 Å and 10 Å peak areas (Esquevin, 1969).

4. Results

4.1. Granulometry

The pattern and composition of sediment records at Sites 1085 and 1087 are relatively equivalent (Fig. 2A, B). The bulk sediment fraction at both sites is composed mainly of fine fraction (<63 μm). Sand fractions are present only in very low amounts with values <5 wt.% at Site 1085 and from 2 to 10 wt.% at Site 1087. The fine fraction is dominated by the clay fraction, which in most cases accounts for 60 to 80 wt.%. According to the classification from Shepard (1954), these sediments exclusively fall in the field of silty clay to clayey silt (Fig. 2C).

The silt fraction is composed mainly of calcareous components (60–80 wt.% of total silt; Fig. 3A). The grain-size distribution of the bulk silt at both sites shows a well-sorted, unimodal, and negatively skewed pattern (Fig. 3A). The mean value at Site 1085 is 3.9 μm (8 Φ), whereas the value at Site 1087 is 4.5 μm (7.8 Φ). Down-core the bulk silt-size distribution pattern at Site 1085 does not exhibit any significant shifting. Interestingly, coarsening trend of bulk silt record is observed at 10.3 and 9.7 Ma at Site 1087 (Fig. 3A).

4.2. Biogenic sedimentation patterns

The $CaCO_3$ concentrations are generally about 10 to 20 wt.% lower at Site 1085 than at Site 1087 (Fig. 4). The carbonate record shows a comparable pattern with the Ca content from Westerhold et al. (2005) (Fig. 5). At both sites, two dramatic drops in carbonate concentration occurred from 10.4 to 10.1 Ma and from 9.6 to 9 Ma (Figs. 4 and 5). At these intervals $CaCO_3$ concentrations decrease to about 25 wt.% at Site 1085 and approximately 60 wt.% at Site 1087. Both decreases are simultaneous with the 'Carbonate Crash' described by Diester-Haass et al. (2004).

The TOC content at both Sites is similar and generally low, ranging from 0.2 to 0.6 wt.% at Site 1085 and from 0.1 to 0.4 wt.% at Site 1087 (Fig. 4). In this study, MAR of TOC and $CaCO_3$ are calculated at Site 1085 only. MAR TOC exhibits a pattern similar to that for TOC concentrations with values lower than 0.06 $g/cm^2/ka$ (Fig. 4). Certain periods are characterized by relatively high variability of TOC content and MAR TOC (e.g., 11.2–10.4 and 10.1–9 Ma), while the rest of the investigated interval displays only minor variation in amplitudes.

The grain-size analysis shows that the calcareous component at both sites is composed predominately of fine silt and clay fraction, with minor sand and coarse calcareous silt (Fig. 6A). Fine silt and clay fraction are composed of calcareous nannoplankton, while the coarse silt and sand fractions consist of foraminifers. The calcareous nannoplankton exhibits high variability down-core and represents the major carbonate share. In this study, we calculate the MAR coccolith by multiplying the fine silt and calcareous clay content by MAR

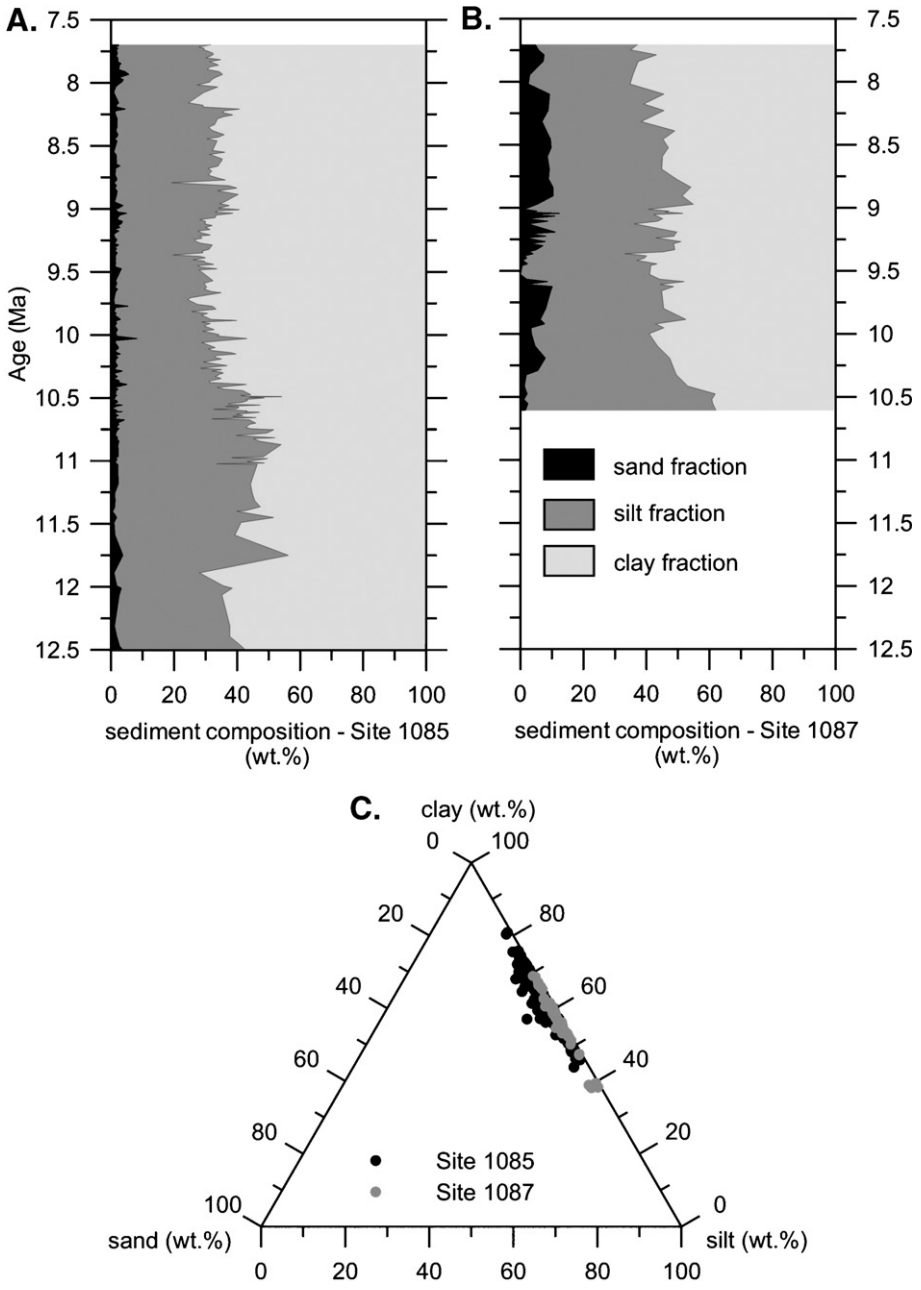

Fig. 2. Temporal variations of the proportions of sediment composition at (A) ODP Site 1085 and (B) Site 1087. (C) Sediment proportion of the ODP Sites 1085 and 1087 in a ternary diagram of the sand, silt, and clay fractions (after the classification of Shepard, 1954).

bulk. Our MAR coccolith record correlates well with the MAR coccolith from Krammer et al. (2006) (Fig. 6B). The MAR coccolith range between 2 and 6 g/cm^2/ka and reveal a comparable pattern with the bulk carbonate content. Some peaks of MAR coccolith value are noted at 11.5 and between 11 and 10.5 Ma. During the middle Miocene the record of fine calcareous silt fraction (2–8 μm) shows a similar pattern to the total carbonate record, but after 10.5 Ma the pattern is relatively constant while the total carbonate content increased.

4.3. Lithogenic sedimentation patterns

The lithogenic components at both sites are dominated by the clay and fine silt fractions (Fig. 7A). The content of terrigenous sortable silt fraction (10–63 μm)

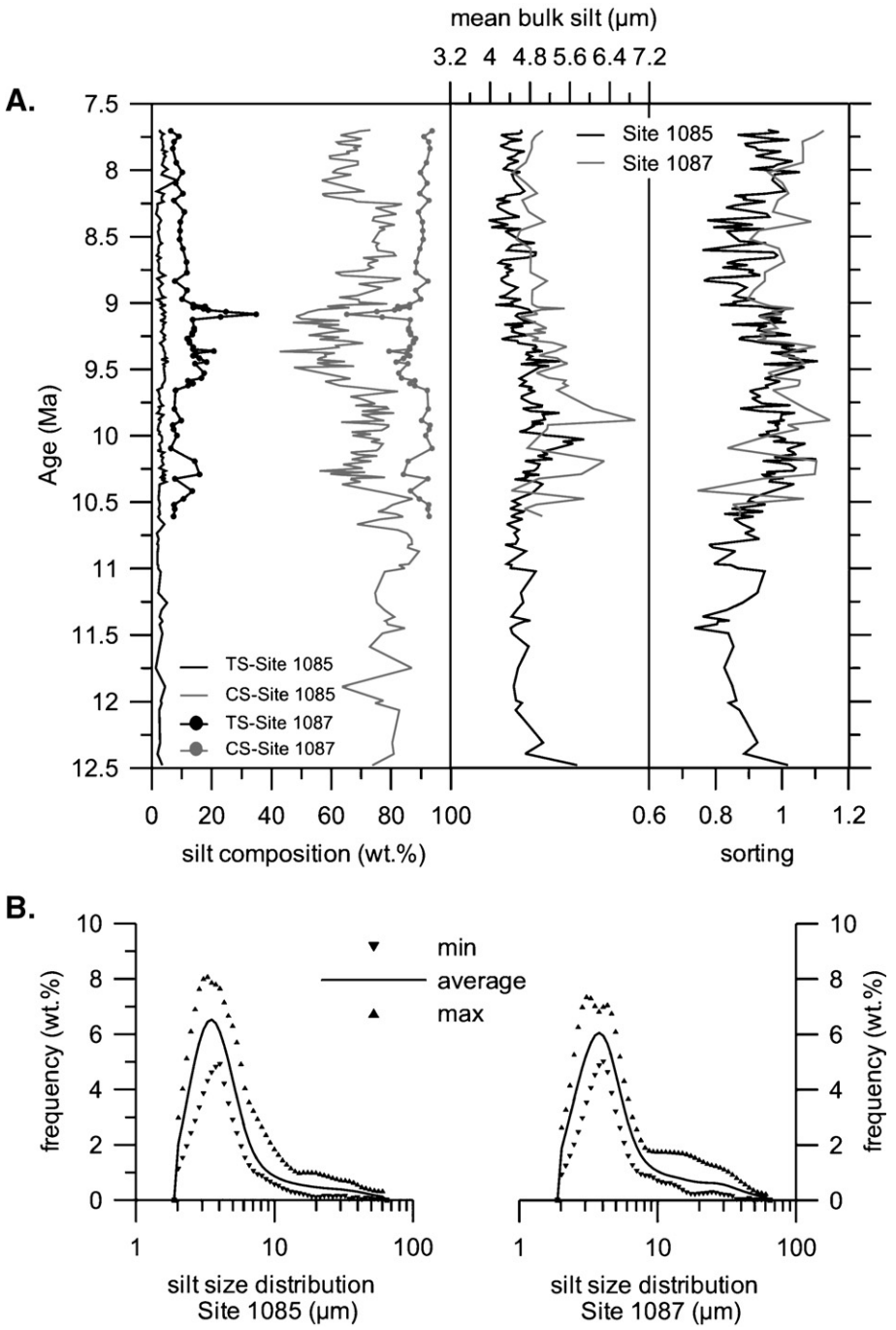

Fig. 3. (A) Temporal variation of composition, mean, and sorting values of the silt fraction at Sites 1085 and 1087 (TS=terrigenous silt fraction, CS=calcareous silt fraction), (B) bulk silt size distribution of Sites 1085 and 1087.

at both sites is low and its variation down-core is independent from LSR and mass accumulation rates of terrigenous components (MARterr) patterns. Some declines in the terrigenous clay fraction, which coincide with a sharp increase in calcareous clay, are well recognized between 11 and 10.5 Ma and between 10.1 and 9.6 Ma. A gradual decrease in terrigenous clay fraction is documented between 9 and 7.5 Ma, with values reaching 10 wt.%. As a common feature, the record of the terrigenous clay fraction at both sites

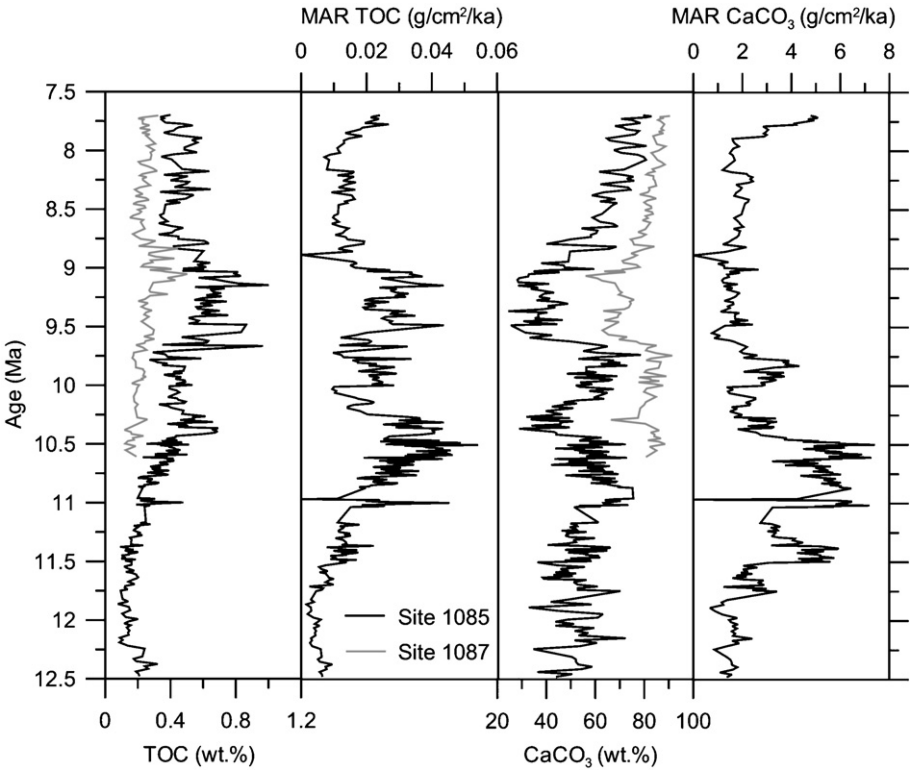

Fig. 4. Temporal variation in concentration of total organic carbon (TOC), mass accumulation rates of TOC (MAR TOC), concentration of carbonate ($CaCO_3$), and mass accumulation rates of carbonate (MAR $CaCO_3$) in sediments from Sites 1085 (black line) and 1087 (grey line).

reveals a similar pattern with the record of Fe content (Westerhold et al., 2005) and pyrite concentration (Diester-Haass et al., 2004).

The MARterr at the studied section, which correlates with the LSR pattern (Fig. 7B), vary between 1 and 5 g/cm^2/ka. The variation of the MARterr is influenced mainly by changes of the MAR of terrigenous clay fraction (MARterr-clay) (Fig. 7A). Some sharp increases of MARterr-clay are observed between 11.5 and 10.2 Ma. These coincide with slight increases in MAR of fine silt (Fig. 7A), which are accompanied by increases in terrigenous matter in 40 to 63 μm fraction, shelf-derived particle and glauconite content (Fig. 7B) according to Diester-Haass et al. (2004).

The general statistic for the terrigenous silt grain-size distribution (mean, average, and maximum) at Sites 1085 (n=215) and 1087 (n=63) are shown in Fig. 8A. It verifies the relatively homogenous and low variability in grain-size composition of the terrigenous silt fraction. Silt analysis at both sites show that terrigenous silt is dominated by the fine-grained fraction (2–10 μm) that ranges from 80 to 85 wt.% of the total silt fraction at Site 1085 and from 70 to 80 wt.% of the total silt fraction at Site 1087, respectively. Grain-size distributions of the fine silt fraction at both sites show unimodal, negatively skewed patterns, and good sorting with a mean value around 3.5 μm (7.8 Φ) at Site 1085 and 5 μm (7.6 Φ) at Site 1087 (Fig. 8B), respectively. Some peaks of the mean terrigenous fine silt values at Site 1087 are distinguished from 11 to 10.5 Ma, 10 to 9.6 Ma, and from 8.5 to 7.5 Ma.

The coarse silt fraction (10–63 μm) exhibits a broad grain-size distribution with size mode at about 5 and 17 μm (Fig. 9A) and gives only small contribution to the silt fraction. The record of terrigenous coarse silt fraction at both sites shows a similar mean value (Fig. 9B), ranging from 15 to 20 μm (5.6–6 Φ). The pattern of mean sortable silt values at Site 1085 down-core displays low variability compared to the record at Site 1087. The mean sortable silt value at Site 1087 shows a coarsening trend from 18 to 20 μm between 10.5 and 10 Ma and between 8.5 and 7.5 Ma. This trend coincides with LSRs and the terrigenous sortable silt content.

4.4. Clay mineralogy

The clay mineralogical study at Site 1085 covers the interval of 9.3 to 7.7 Ma, showing that the clay mineral

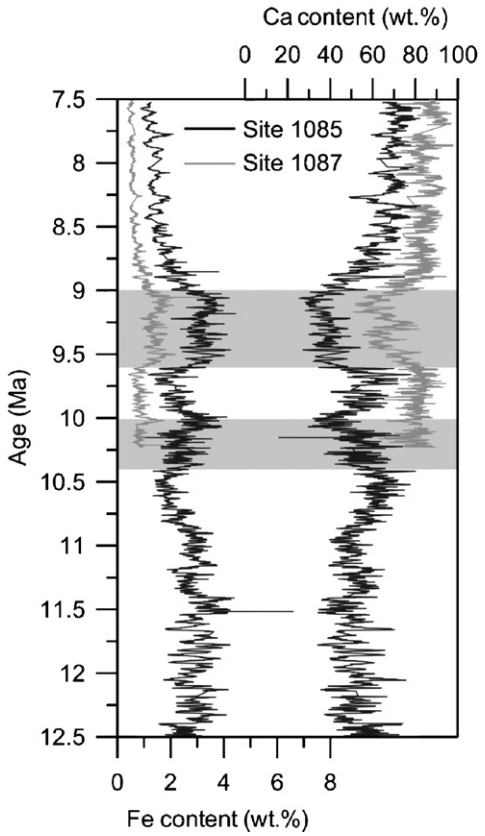

Fig. 5. Temporal variations of the calcium and iron contents at ODP Sites 1085 and 1087 (Westerhold et al., 2005). Grey bars indicate Miocene 'carbonate crash' event.

assemblage during the late Miocene is dominated by illite (50% to 60%) with minor contribution of smectite (20% to 30%) and equal proportions of chlorite and kaolinite (8% to 10%) (Fig. 10). Illite chemistry (the 5/10 Å ratio) in the whole studied section shows a values >0.5, pointing to Al-rich illite (Gingele, 1996). Clay mineralogy is characterized by decreasing smectite content and slightly increasing kaolinite and illite contents. A decrease in the S/I ratio and smectite contents is mirrored by illite chemistry.

5. Discussion

5.1. Long-term modes and major shifts in sedimentation patterns

The biogenic component in the study areas is dominated by carbonate content that shows several sharp decreases between 10.4 and 10.1 Ma and between 9.6 and 9.0 Ma. Calcareous component found in the samples of Sites 1085 and 1087 are characterized by abundant calcareous nannofossils with very low amounts of foraminifers (Fig. 6A) which indicate prevailing nannoplankton productivity under oligotrophic conditions at temperate to warm sea-surface temperatures (Burckle et al., 1996). This is in good agreement with results from the same time interval at ODP Sites 1088 and 1092 in the Atlantic sector of the Southern Ocean presented by Diekmann et al. (2003). The changes in relative abundance of the coarse fraction may in general reflect (1) ecological factors (Bassinot et al., 1994), or (2) sedimentological factors, such as carbonate dissolution (Berger et al., 1982) or changes in dilution by fine-grained, nonbiogenic particles. The overall relatively constant and low amounts of MAR of foraminifers suggest that there are no significant changes in carbonate production. Enhanced carbonate dissolution should increase the benthic/planktic (B/P) foraminifers ratio. No significant correlation was detected between changes in B/P ratios between 12 and 9 Ma and with decreases in carbonate content at Site 1085 led Diester-Haas et al. (2004) to conclude that dissolution is not a major process controlling the minima in carbonate content that correspond in time to the global 'Carbonate Crash'.

Our grain-size distribution of the terrigenous component is dominated by the fine-silt fraction. According to the classification of Höppner and Henrich (1999), the sediment was grouped as accumulated sediment transported by suspension. The lower variation of mean terrigenous coarse silt values at Site 1085 compared to Site 1087 is due to its location relatively near to the sediment source from the Orange River.

The composite terrigenous fraction can be assembled by various sources and different processes. At the Southwest African continental margin, the Orange River discharge and aeolian input from the Namib Desert are the main sources supplying terrigenous material (Gingele, 1996). Several grain-size studies stress the possibility to use the grain-size distribution pattern from deep-sea cores to determine the relative abundance of sediments deposited by hemipelagic and aeolian processes (e.g., Boven and Rea, 1998; Holz et al., 2004; Koopmann, 1981; Rea and Hovan, 1995; Stuut et al., 2002, Stuut and Lamy, 2004). The grain size of the aeolian particles in deep-sea sediments depends on distance to the source and the capacity of the transporting agents. Close to the continent, the sediments are generally coarser grained compared with the distal open ocean. Most deep-sea cores recovered within hundreds of kilometers off continents are characterized by fine-grained aeolian dust (2–4 μm; e.g., Boven and Rea, 1998; Rea and Hovan, 1995), while several deep-

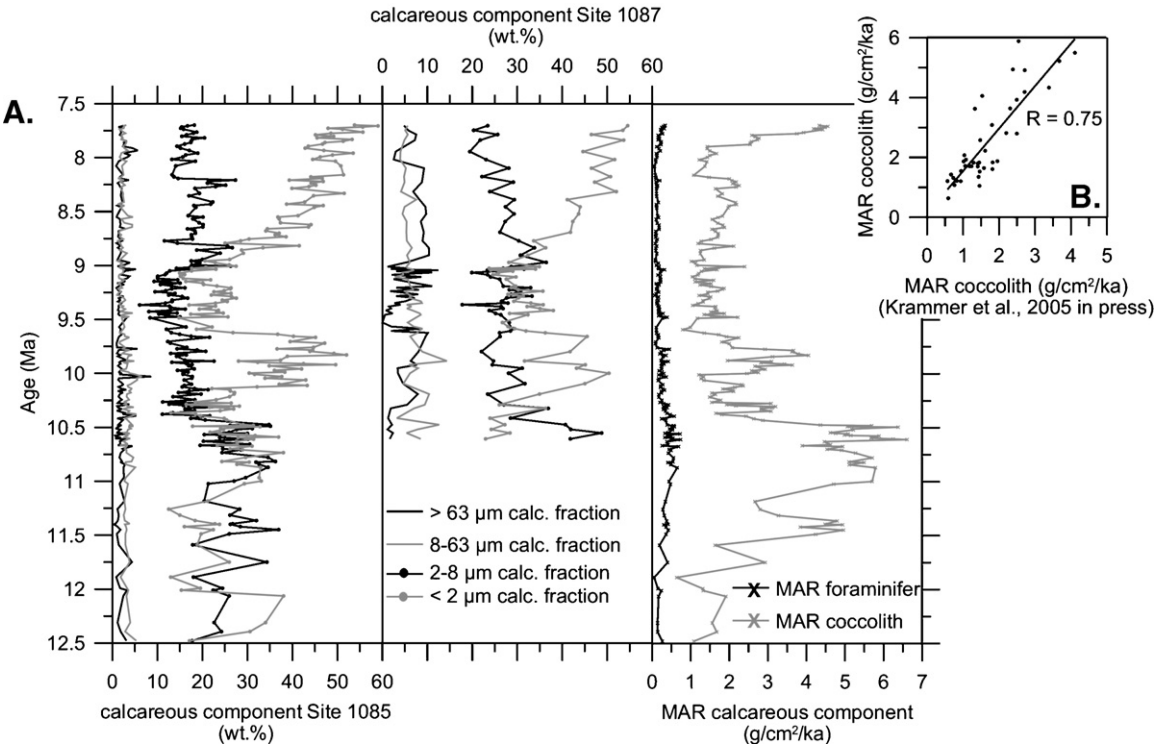

Fig. 6. (A) Temporal variation in calcareous components in sediments at Sites 1085 and 1087 and mass accumulation rates of foraminifers and coccoliths; (B) mass accumulation rate of calcareous nannoplankton calculated from the calcareous fine fraction (<8 µm) and of coccolith carbonate based on coccolith individuals (Krammer et al., 2006) from the same samples.

sea sediment studies located relatively close to the continent showed that aeolian dust fallout is characterized by terrigenous sediment with a modal grain size larger than 6 µm (e.g., Koopmann, 1981; Holz et al., 2004; Moreno et al., 2002; Stuut et al., 2002). This is supported by the coarse silt sized of present-day dust samples from the Namib Desert collected along transect from the coast to the core Site at MD 962094, Walvis Ridge (Stuut et al., 2002). Since the studied sites are located relatively close (few hundreds of kilometers) to the source of the wind-blown sediment, the coarse silt fraction is interpreted as aeolian origin and the fine silt to clay fractions is related to erosion and run off from the Orange River.

Interestingly, the mean size of terrigenous sortable silt could also be used as an indicator of relative bottom current strength (McCave et al., 1995b). Following these interpretations, we assume that terrigenous sortable silt variability at the study area may be used as an indicator of paleo bottom-current strength and/or dust supply derived from the Namib Desert. The similar grain-size patterns in both coarse calcareous (10–63 µm) and terrigenous sortable silt fractions during a period from 11.7 to 11 Ma point to a common grain-size sorting process that can only be achieved through common current sorting and grain-size selection by bottom-water circulation (Robinson and McCave, 1994) (Fig. 9B). On the other hand, independent granulometric signals in the biogenic and lithogenic fractions during 11 to 7.5 Ma reflect primary and granulometrically unmodified sediment input by biological export production and aeolian supply. Thus, the terrigenous sortable silt in this interval is possibly controlled by dust input (Fig. 9B).

The middle to late Miocene records of high terrigenous clay and fine silt fluxes from both sites imply stronger terrigenous input that probably correspond to periods of enhanced moisture in, and runoff from the hinterland and/or an increase in delivery of clastic material caused by a sea level regression that shifted the river mouth closer to the shelf edge (e.g., Haq et al., 1987).

5.2. Interplay of terrigenous versus biogenic sedimentation: middle to early late Miocene (12.5–10.5 Ma)

In this period only sediment samples from Site 1085 have been analyzed. The magnetic susceptibility values

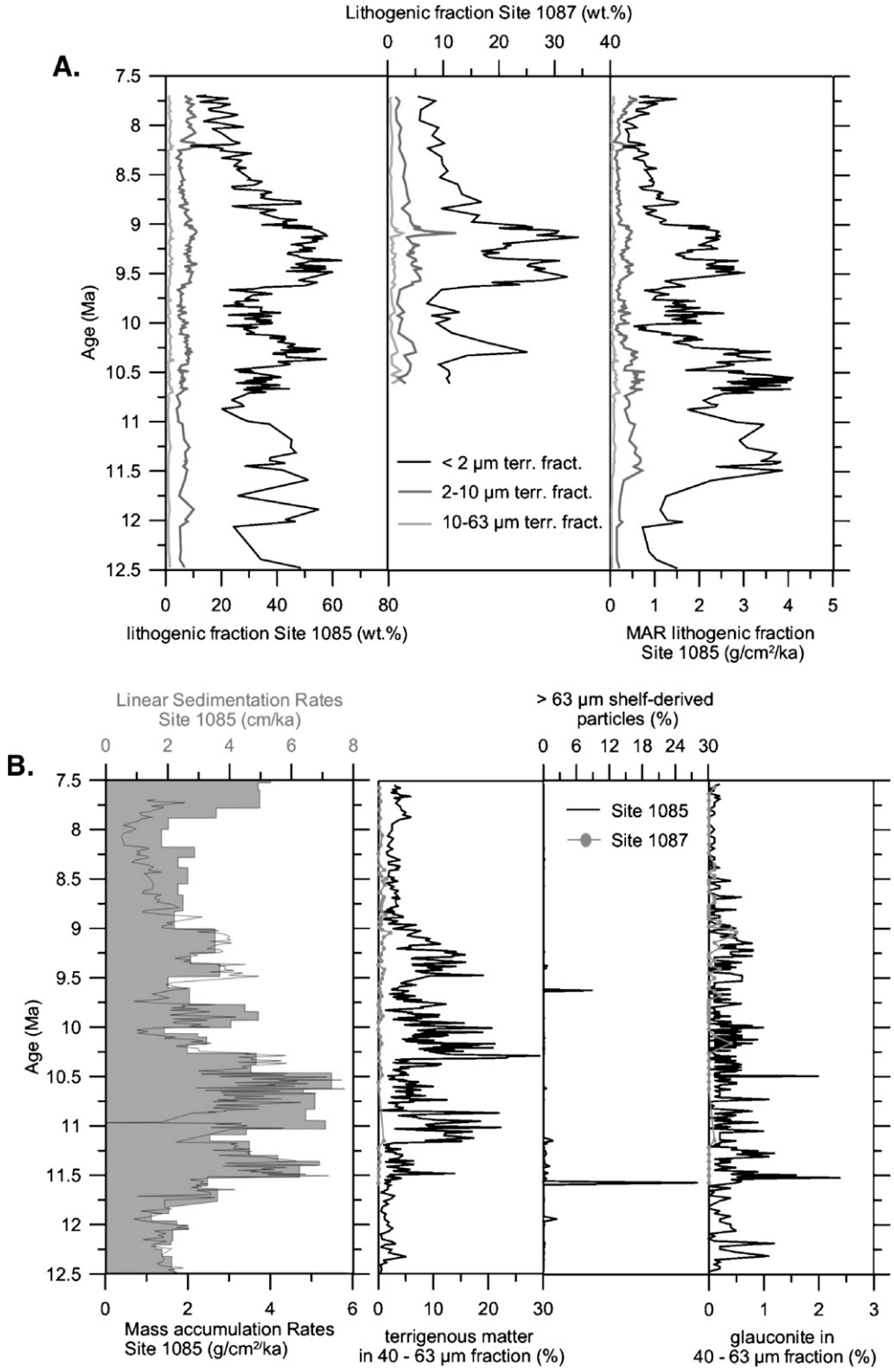

Fig. 7. Temporal variations in (A) composition of lithogenic fraction and mass accumulation rates of each terrigenous fraction in sediments from Sites 1085 and 1087; (B) linear sedimentation rates and mass accumulation rates of terrigenous component (Westerhold et al., 2005), contribution of terrigenous material (%) of the total 40–63 µm fraction, concentration of shelf derived particles in the sand fraction, and glauconite in the 40–63 µm fraction (from Diester-Haass et al., 2004).

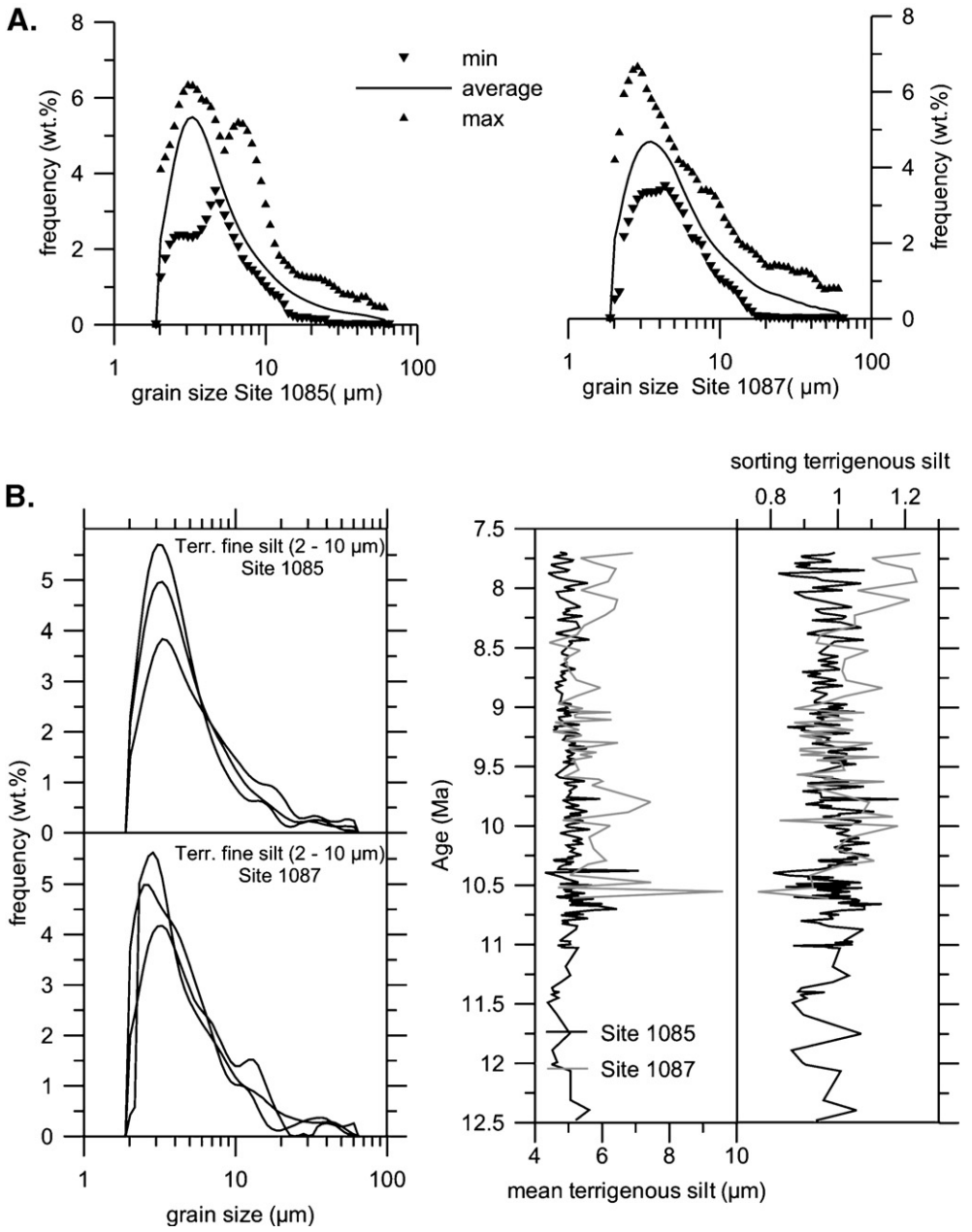

Fig. 8. (A) Statistics of terrigenous silt-size distribution at Sites 1085 ($n=215$) and 1087 ($n=63$); maximum, average, and minimum frequency record; (B) grain-size distribution of terrigenous fine silt (2–63 µm), mean value, and sorting at Site 1085 and Site 1087.

of sediments from Site 1085 increase during this period (Wefer et al., 1998), pointing to increases in the amount of clastic components. This period shows two different intervals, including low LSR and low MARterr from 12.5 to 11.7 Ma, which is followed by a sharp rise in both parameters and terrigenous clay content. As mentioned above, the sortable silt record during this period can be used as indicator for bottom current activity and dust supply. At 11.7 Ma high content and coarse mean of terrigenous sortable silt (Fig. 9B), which indicates an increase in bottom current activity, are associated with major peaks of Fe content (Fig. 6B), coarse (40–63 µm) terrigenous matter concentrations, and shelf-derived particles (Diester-Haass et al., 2004). These series of events coincide with an increasing trend of the benthic $\delta^{18}O$ at ODP Site 1085 (Westerhold et al., 2005), pointing to a cooling trend and an expansion of the Antarctic ice sheet that would induce a lowering of

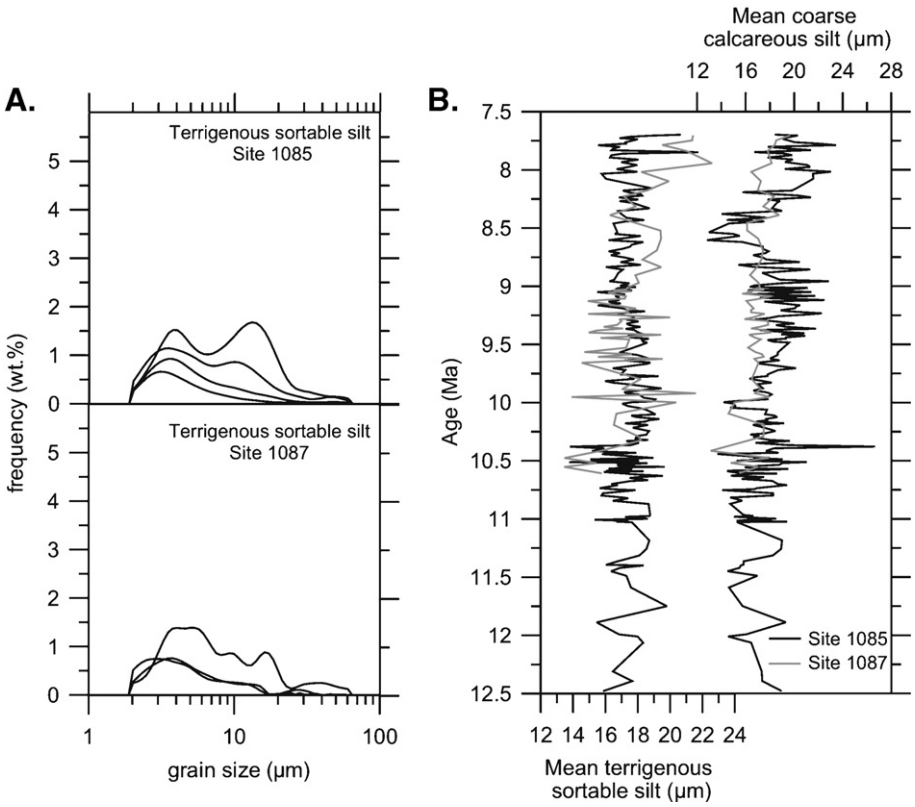

Fig. 9. (A) Grain size distribution of terrigenous sortable silt (10–63 μm) at Sites 1085 and 1087. (B) Comparison between the mean grain diameters of the terrigenous sortable silt (terrigenous coarse silt) with the mean grain diameter of coarse calcareous silt (10–63 μm), following Robinson and McCave (1994).

the sea level. As postulated by Diester-Haass et al. (2004), an increase in bottom current activity at 11.7 Ma might be related to the strong erosion of the shelf resulting in transport of sediment loads to the continental slope due to sea-level regression.

The biogenic carbonate record in this interval shows an increasing trend of MAR coccolith that reaches the highest value at 10.5 Ma, indicating a high calcareous nannoplankton export production. Interestingly the small sized placolith (reticulofenestrids; Krammer et al., 2006), which is a good indicator for high productivity environment, is relatively low and constant during 12.5 to 11.2 Ma, suggesting that the Benguela upwelling system and its wind-driven atmospheric forcing did not yet exist during this time interval.

An increase in calcareous clay content after 11.2 Ma, which is accompanied by an increase in MAR coccolith, and terrigenous sortable silt content as well as a coarsening in mean terrigenous sortable silt value might possibly related to the expansion of East Antarctic ice-sheets that supply the cool intermediate waters to mid-latitude surface waters in the upwelling regions and established the initiation of the Benguela upwelling system (Siesser, 1978). According to Diester-Haass et al. (2004), paleoproductivity, mass accumulation rates, the number of benthic foraminifers and benthic foraminiferal accumulation rates began to increase at 12 Ma at Site 1085. This would signify an earlier onset of upwelling as compared to the datum indicated by the grain-size distribution at about 11.2 Ma.

5.3. Interplay of terrigenous versus biogenic sedimentation: early to middle late Miocene (10.5–9 Ma)

This time interval is characterized by two major depressions in carbonate content, which occur from 10.4 to 10.1 and from 9.6 to 9.0 Ma. They are simultaneous with the “Carbonate Crash” event in the equatorial Pacific Ocean (Lyle et al., 1995). So far, these major drops are assumed to be caused either by dilution from major increases in clastic input from the shelf during a global sea level regression (Diester-Haass et al., 2004) or by changes in nannoplankton production (Krammer et al., 2006).

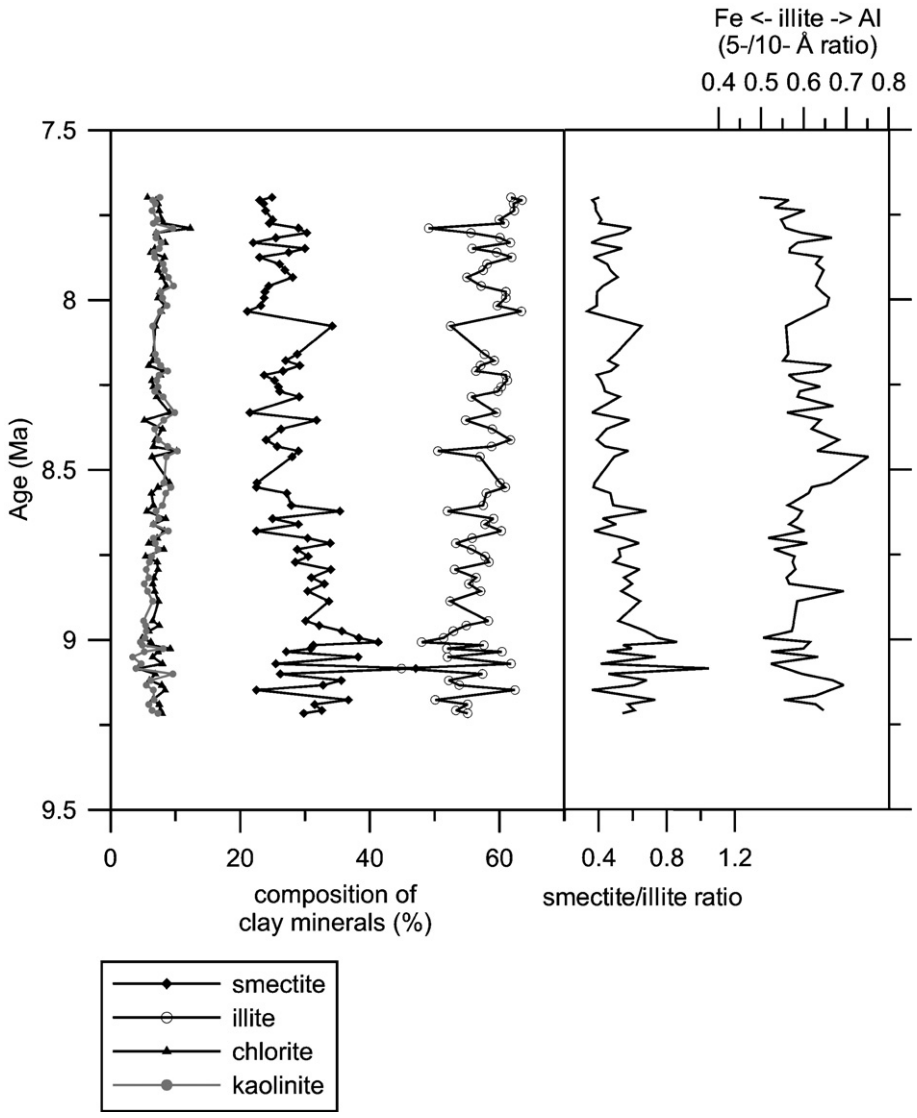

Fig. 10. Temporal variation of clay mineral composition at Site 1085.

Our data show that at the interval between 10.4 and 10.1 Ma, the drops in carbonate content coincide with the strongly decreasing MAR coccolith. If this decrease was controlled by dilution, it should be accompanied by an increase in lithogenic component. In contrast, our MARterr and the LSR records show a decreased pattern. This is comparable with the terrigenous coarse silt record, which shows no significant changes in content and mean value. Accordingly, this time interval is also characterized by a very low content of shelf-derived particles (Diester-Haass et al., 2004). Therefore, we propose that the drop of $CaCO_3$ concentration at this time interval is not controlled by dilution. This is in good agreement with the results of the recent study of Krammer et al. (2006), identifying the changes in coccolith production as the major controlling process on $CaCO_3$ concentration.

The depression of biogenic carbonate content at the interval between 9.6 and 9 Ma is characterized by high amounts of lithogenic components, as well as high MARterr and LSR. This is accompanied by significant amount of shelf-derived particles (Diester-Haass et al., 2004) at 9.6 Ma. At the same time, MAR coccolith shows a strong decrease from 4 to 1 g/cm^2/ka, indicating a weakening of small placolith production. Therefore, we assume that the declines in $CaCO_3$ concentration between 9.6 and 9 Ma are caused by a combination of weakening of coccoliths production and dilution, due to

a sea-level regression that shifted the river mouth closer to the shelf edge and transported the terrigenous material from the shelf into the ocean (e.g., Diester-Haass et al., 2004; Haq et al., 1987).

Additionally, this interval (10.5–9 Ma) is characterized by an increase in terrigenous sortable silt content and clear coarsening trend at 10.5 Ma, especially at Site 1087. According to the scheme of Robinson and McCave (1994), the pattern of the terrigenous sortable silt is related to an increase in dust input. This timing may generally be linked to the intensification of upwelling in the studied region, which is paralleled with the results based on nannofossil studied from Krammer et al. (2006), and the aridification as a result from strengthened southeastern trade winds (Siesser, 1980; Diester-Haass et al., 1990, 1992).

5.4. Interplay of terrigenous versus biogenic sedimentation: middle late Miocene (9–7.5 Ma)

The middle late Miocene is characterized by a gradual decrease in terrigenous clay and Fe contents together with a decrease in MARterr (Fig. 7A). This is accompanied by clay mineralogical data that shows a decrease in smectite content. The Cape province is known as a source of smectite, as the weathering products of the Karoo lavas in the upstream areas of the Orange River, as well as the highland plateau of Angola drained via the Kunene River (Gingele, 1996; Robert et al., 2005). Therefore, smectite at Site 1085 can be considered as a tracer for run-off and climate in the Orange drainage basin. Moreover, illite 5/10 Å ratios at Site 1085 are overall above 0.5, representing strong hydrolysis process (Gingele, 1996; Petschick et al., 1996). The presence of smectite and aluminum-bearing illite in this site indicate riverine input. Since Site 1085 is strongly influenced by fluvial input due to its proximity to the river mouth, the decreases of terrigenous silt and total clay contents as well as smectite concentration might be used as an indicator of a weakening in fluvial input. This is possibly related to continental aridity.

Interestingly, the terrigenous silt records at both sites exhibit a different pattern. The mean terrigenous silt value at Site 1085 remains constantly fine (Fig. 8B). In contrast, Site 1087, which is located relatively far from the Orange River mouth, shows a significant coarsening in mean values and increasing content of terrigenous sortable silt without a significant increase of LSR and MARterr. This might be linked to a strengthening of dust supply and an intensification of the southeastern trade winds. This is parallel with biogenic record which reveals an increase in small placolith abundance (Fig. 6A) during this interval, signifying the presence of

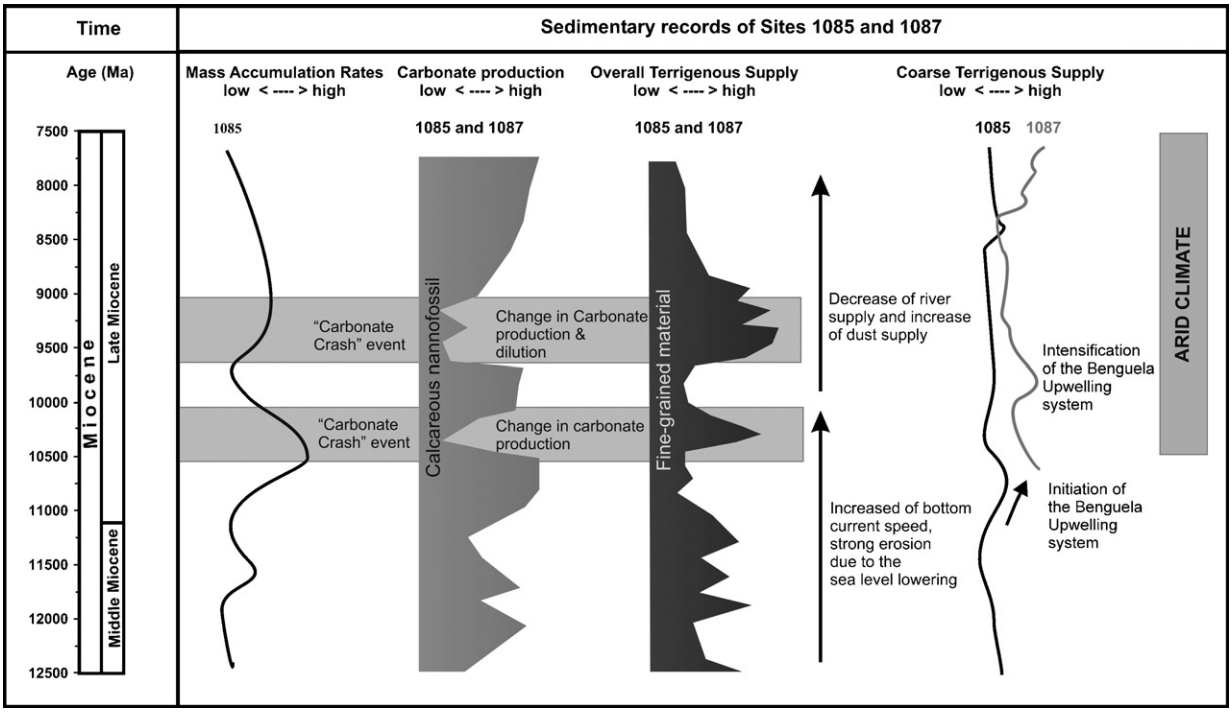

Fig. 11. Summary of the sediment records of Sites 1085 and 1087 and their interpretations.

cooler surface water at the study area (Krammer et al., 2006) that strengthens the upwelling. This finding is consistent with the intensification of the upwelling system and aridification of Southwest Africa (Partridge, 1993).

6. Summary and conclusion

This study presents the results of compositional ($CaCO_3$ and TOC), clay mineralogical, and grain-size investigations (sand/silt/clay proportions and terrigenous silt grain-size distribution) on a set of middle to late Miocene sediment samples from the SW African continental margin. These identify changes in regional climate and paleoceanography of the southeastern Atlantic during the middle to the late Miocene (Fig. 11). The establishment of the wind-driven Benguela upwelling system occurred at 11.2 Ma, which is indicated by an increase in TOC content together with an increase in coarse terrigenous silt content and coarsening trend. Significant drop of $CaCO_3$ concentration between 10.4 and 10.1 Ma is caused mainly by variation in calcareous nannoplankton production, whereas drop of $CaCO_3$ concentration between 9.6 and 9 Ma is controlled mainly by a combination of changes in calcareous nannoplankton production and dilution.

During the late Miocene, river input processes became weak, which is evident from a decrease of fine silt and smectite contents, whereas the dust input became stronger, pointing to the intensification of wind-driven Benguela upwelling system and period of aridity in the hinterland.

Acknowledgements

We would like to thank L. Diester-Haass, for sharing her data on shelf-derived components with us. T. Westerhold provided the isotope and XRF-core scanner dataset. We also thank T. Bickert, B. Beckmann and R. Krammer for their valuable discussion and suggestion in reviewing the manuscript. We thank Helga Heilmann and Brit Kockisch for laboratory and technical assistance. We gratefully acknowledge thoughtful comments from P. Meyers and one anonymous reviewer. We thank the Ocean Drilling Program for providing samples. This study was funded by the Deutsche Forschungsgemeinschaft (DFG Research Center Ocean Margins). This is RCOM publication no. RCOM0405.

References

Bassinot, F.C., Beaufort, L., Vincent, E., Labeyrie, L.D., Rostek, F., Müller, P.J., Quidelleur, X., Lancelot, Y., 1994. Coarse fraction fluctuation in pelagic carbonate sediments from the tropical Indian Ocean: A 1500 ky record of carbonate dissolution. Paleoceanography 9, 579–600.

Berger, W.H., 1989. Global maps of ocean productivity. In: Berger, H.W., Smetacek, V.S., Wefer, G. (Eds.), Productivity in the Ocean: Present and Past, Dahlem Conf. John Wiley, Chichester, pp. 429–455.

Berger, W.H., Bonneau, M.-C., Parker, F.L., 1982. Foraminifera on the deep-sea floor: lysocline and dissolution rate. Oceanologica Acta 5, 249–258.

Biscaye, P.E., 1965. Mineralogy and sedimentation of recent deep-sea clay in the Atlantic Ocean and adjacent seas and oceans. Gological Society of America Bulletin 76, 803–832.

Boven, K.L., Rea, D.K., 1998. Partition of eolian and hemipelagic sediment in eastern Equatorial Pacific core TR 163–31B and the late Quaternary Paleoclimate of the Northern Andes. Journal of Sedimentary Research 68, 850–855.

Bremner, J.M., 1978. Sediments on the continental margin off South West Africa between latitude 17° and 25°S. Thesis. Geol. Dep., University of Cape Town, pp. 300.

Burckle, L.H., Mortlock, R., Rudolph, S., 1996. No evidence for extreme, long term warming in early Pliocene sediments of the Southern Ocean. Marine Micropaleontology 27, 215–226.

Chester, R., Elderfield, H., Griffin, J.J., 1971. Dust transported in the north-east and south-east trade winds in the Atlantic Ocean. Nature 233, 474–476.

Chester, R., Elderfield, H., Griffin, J.J., Johnson, L.R., Padgham, R.C., 1972. Aeolian dust along the eastern margins of the Atlantic Ocean. Marine Geology 13, 91–105.

Diekmann, B., Fälker, M., Kuhn, G., 2003. Environmental history of the south-eastern South Atlantic since the middle Miocene: evidence from the sedimentological records of ODP Sites 1088 and 1092. Sedimentology 50, 511–529.

Diester-Haass, L., Meyers, P.A., Rothe, P., 1990. Miocene history of the Benguela Current and Antarctic ice volumes: evidence from rhythmic sedimentation and current growth across the Walvis Ridge (DSDP Sites 362 and 532). Paleoceanography 5, 685–707.

Diester-Haass, L., Meyers, P.A., Rothe, P., 1992. The Benguela current and associated upwelling on the southwest African Margin: a synthesis of the Neogene–Quaternary sedimentary record at DSDP Sites 362 and 532. In: Prell, C.P., Emeis, K.C. (Eds.), Upwelling Systems: Evolution Since the Early Miocene. Geological Society Special Publication, pp. 331–342.

Diester-Haass, L., Meyers, P.A., Bickert, T., 2004. Carbonate crash and biogenic bloom in the late Miocene: evidence from ODP Sites 1085, 1086 and 1087 in the Cape Basin, southeast Atlantic Ocean. Paleoceanography 19 (1), 1–19.

Esquevin, J., 1969. Influence de al composition chimique des illites sur cristallinite. Bulletin du Centre de Recherches Pau-SNPA 3 (1), 147–153.

Farrel, J.W., Rafii, I., Janecek, T.R., Murray, D.W., Levitan, M., Dadey, K.A., Emeis, K.-C., Lyle, M., Flores, J.-A., Hovan, S., 1995. Late Neogene sedimentation patterns in the eastern equatorial Pacific Ocean. Proceedings ODP, Science Results, vol. 138. Ocean Drilling Program, College Station, TX, pp. 717–753.

Flower, B.P., Kennet, J.P., 1995. Middle Miocene deep water paleoceanography in the southwest Pacific: relations with East Antarctic Ice Sheet development. Paleoceanography 10 (6), 1095–1112.

Frenz, M., Baumann, K.H., Boeckel, B., Hoeppner, R., Henrich, R., 2005. Quantification of foraminifer and coccolith carbonate in South Atlantic surface sediments by means of carbonate grain-

size distribution. Journal of Sedimentary Research 75, 468–479.

Gingele, F.X., 1996. Holocene climatic optimum in Southwest Africa – evidence from the marine clay mineral record. Palaeogeography, Palaeoclimatology, Palaeoecology 122, 77–87.

Haq, B.U., Hardenbol, J., Vail, P.R., 1987. Chronology of fluctuating sea levels since the Triassic. Science 235, 1156–1166.

Hay, W.W., Brock, J.C., 1992. Temporal variations in intensity of upwelling off southwest Africa. In: Summerhayes, C.P., Prell, W.L., Emeis, K.C. (Eds.), Upwelling Systems: Evolution Since the Early Miocene. Geological Society Special Publication, pp. 463–497.

Holz, C., Stuut, J.B.W., Henrich, R., 2004. Terrigenous sedimentation processes along the continental margin off NW Africa: implications from grain-size analysis of seabed sediments. Sedimentology 51, 1145–1154.

Höppner, R., Henrich, R., 1999. Kornsortierungsprozesse am Argentinischen kontinentalhang anhand von Siltkorn-Analysen. Zborník Geologických Palaeontologie Teil I, 897–905.

Kennett, J.P., Keller, G., Srinivasan, M.S., 1985. Miocene planktonic foraminiferal biogeography and paleoceanography development of the Indo-Pacific Region. In: Kennett, J.P (Ed.), The Miocene Ocean: Paleoceanography and Biogeography. Geological Society of America Memoir, 163, pp. 197–263.

King, T.A., Ellis, J., Murray, W.G., Shackleton, N.J., Harris, S., 1997. Miocene evolution of carbonate sedimentation at the Ceara Rise: a multivariate data/proxy approach. In: Shackleton, N.J., Curry, W. B., Richter, C., Bralower, T.J. (Eds.), Proceedings ODP, Science Results, vol. 154. Ocean Drilling Program, College Station, TX, pp. 349–364.

Koopmann, B., 1981. Sedimentation von Saharastaub im subtropischen Nordatlantik wahrend der letzen 25.000. Jahres Meteorology Forschsergeb. 35, 23–59.

Krammer, R., Baumann, K.-H., Henrich, R., 2006. Middle to late Miocene fluctuations in the incipient Benguela upwelling system revealed by coccolith assemblages (ODP Site 1085A). Palaeogeography, Palaeoclimatology, Palaeoecology 230 (3–4), 319–334.

Lyle, M., Dadey, K.A., Farrel, J.W., 1995. The late Miocene (11–8 Ma) eastern Pacific carbonate crash: evidence for reorganization of deep-water circulation by the closure of the Panama gateway. In: Pisias, N.G., Mayer, L.A., Janecek, T.R., Palmer-Julson, J., van Andel, T.H. (Eds.), Proceedings ODP, Science Results, vol. 138. Ocean Drilling Programm, College Station, TX, pp. 821–838.

McCave, I.N., Manighetti, B., Beveridge, N.A.S., 1995a. Circulation in the glacial North Atlantic inferred from grain-size measurement. Nature 374, 149–151.

McCave, I.N., Manighetti, B., Robinson, S.G., 1995b. Sortable silt and fine sediment size composition slicing: parameters for palaeocurrent speed and palaeoceanography. Paleoceanography 10, 593–610.

Moreno, A., Cacho, I., Canals, M., Prins, M.A., Sanchez-Goni, M.-F., Girimalt, J.O., Weltje, T.J., 2002. Saharan dust transport and high-latitude glacial climate variability: the Aboran Sea record. Quaternary Research 58, 318–328.

Partridge, T.C., 1993. The evidence for Cainozoic aridification in Southern Africa. Quaternary International 17, 105–110.

Peterson, R.G., Stramma, L., 1991. Upper-level circulation in the South Atlantic Ocean. Progress in Oceanography 26, 1–73.

Petschick, R., Kuhn, G., Gingele, F.X., 1996. Clay mineral distribution in surface sediments of the South Atlantic: sources, transport, and relation to oceanography. Marine Geology 130, 203–229.

Rea, D.K., Hovan, S.A., 1995. Grain size distribution and depositional processes of the mineral component of abyssal sediments: lesson from the North Pacific. Paleoceanography 10, 251–258.

Robert, C., Diester-Haass, L., Paturel, J., 2005. Clay mineral assemblages, siliciclastic input and paleoproductivity at ODP Site 1085 off Southwest Africa: a late Miocene–early Pliocene history of Orange River discharges and Benguela current activity and their relation to global sea level change. Marine Geology 216, 221–238.

Robinson, S.G., McCave, I.N., 1994. Orbital forcing of bottom current enhanced sedimentation on Feni Drift, NE Atlantic, during the Mid Pleistocene. Paleoceanography 9, 943–972.

Rogers, J., 1977. Sediments on the continental margin off the Orange River and the Namib Desert. PhD. Thesis, Geological Department, University of Cape Town, p. 212. unpublished.

Roth, M.J., Droxler, A.W., Kameo, K., 2000. The Caribbean carbonate crash at the middle to late Miocene transition: linkage to the establishment of the modern global ocean conveyor. In: Leckie, R. M., Sigursson, H., Acton, G.D., Draper, G. (Eds.), Proceedings ODP, Science Results, vol. 165. Ocean Drilling Program, College Station, TX, pp. 249–273.

Shepard, H.P., 1954. Nomenclature based on sand–silt–clay ratios. Journal of Sedimentary Petrology 34, 151–158.

Siesser, W.G., 1978. Aridification of the Namib Desert: evidence from oceanic core. In: van Zinderen-Bakker (Ed.), Antarctic Glacial History and World Paleoenvironment. Balkema, Rotterdam, pp. 105–112.

Siesser, W.G., 1980. Late Miocene origin of the Benguela upwelling system off Northern Namibia. Science 208, 283–285.

Stuut, J.B.W., Prins, M.A., Schneider, R.R., Weltje, G.J., Jansen, J.H. F., Postma, G., 2002. A 300-kyr record of aridity and wind strength in southwestern Africa: inferences from grain-size distributions of sediments of Walvis Ridge, SE Atlantic. Marine Geology 180, 221–233.

Stuut, J.B.W., Lamy, F., 2004. Climate variability at the southern boundaries of the Namib (southwestern Africa) and Atacama (northern Chile) coastal deserts during the last 120,000 yr. Quaternary Research 62, 301–309.

Summerhayes, C.P., Kroon, D., Rosell-Mel, A., Jordan, R.W., Schrader, H.-J., Hearn, R., Vilanueva, J., Grimalt, J.O., Englington, G., 1995. Variability in the Benguela Current upwelling system over the past 70.000 years. Progress in Oceanography 35, 207–251.

Van der Merwe, C.R., Heystek, H., 1955. Clay minerals of South African soul groups: Part III. Soils of the desert and adjoining semi-arid regions. Soil Science 80, 479–494.

Wefer, G., Berger, W.H., Richter, C., et al., 1998. Proc. ODP, Init. Reports, vol. 175. Ocean Drilling Programm, College Station, TX. 1477 pp.

Westerhold, T., Bickert, T., Röhl, U., 2005. Middle to late Miocene Oxygen Isotope Stratigraphy of ODP Site 1085 (SE Atlantic): new constrains on Miocene climate variability. Palaeogeography, Palaeoclimatology, Palaeoecology 217, 205–222.

Wright, J.D., Miller, K.G., 1996. Control of North Atlantic deep water circulation by the Greenland Scotland Ridge. Paleoceanography 11, 157–169.

Zachos, J.C., Pagani, M., Sloan, L., Thomas, E., Billups, K., 2001a. Trends, rhythms, and aberrations in global climate 65 Ma to present. Science 292, 686–693.

Zachos, J.C., Shackleton, N.J., Evenaugh, J.S., Pallike, H., Flower, B.P., 2001b. Climate response to orbital forcing across the Oligocene–Miocene boundary. Science 292, 274–278.